Determination of Rayleigh wave ellipticity across the Earthscope Transportable Array using single-station and array-based processing of ambient seismic noise

Eli Workman,* Fan-Chi Lin and Keith D. Koper

Department of Geology and Geophysics, the University of Utah, Salt Lake City, UT 84112, USA. E-mail: Workman.Eli@ensco.com

SUMMARY
We present a single station method for the determination of Rayleigh wave ellipticity, or Rayleigh wave horizontal to vertical amplitude ratio (H/V) using Frequency Dependent Polarization Analysis (FDPA). This procedure uses singular value decomposition of 3-by-3 spectral covariance matrices over 1-hr time windows to determine properties of the ambient seismic noise field such as particle motion and dominant wave-type. In FPDA, if the noise is mostly dominated by a primary singular value and the phase difference is roughly 90° between the major horizontal axis and the vertical axis of the corresponding singular vector, we infer that Rayleigh waves are dominant and measure an H/V ratio for that hour and frequency bin. We perform this analysis for all available data from the Earthscope Transportable Array between 2004 and 2014. We compare the observed Rayleigh wave H/V ratios with those previously measured by multicomponent, multistation noise cross-correlation (NCC), as well as classical noise spectrum H/V ratio analysis (NSHV). At 8 s the results from all three methods agree, suggesting that the ambient seismic noise field is Rayleigh wave dominated. Between 10 and 30 s, while the general pattern agrees well, the results from FDPA and NSHV are persistently slightly higher (∼2 per cent) and significantly higher (>20 per cent), respectively, than results from the array-based NCC. This is likely caused by contamination from other wave types (i.e. Love waves, body waves, and tilt noise) in the single station methods, but it could also reflect a small, persistent error in NCC. Additionally, we find that the single station method has difficulty retrieving robust Rayleigh wave H/V ratios within major sedimentary basins, such as the Williston Basin and Mississippi Embayment, where the noise field is likely dominated by reverberating Love waves and tilt noise.

Key words: Time-series analysis; Surface waves and free oscillations; Site effects; Seismic tomography; North America.

1 INTRODUCTION

The horizontal to vertical spectral noise ratio (H/V ratio) (Nakamura 1989) has often been used to study site amplification and shallow crustal structure and has been particularly helpful in seismic hazard assessment (e.g. Field & Jacob 1993; Bonila *et al.* 1997; Konno & Ohmachi 1998; Riepl *et al.* 1998; Parolai *et al.* 2002; Bonnefoy-Claudet *et al.* 2006). However, the H/V ratio can be influenced by the composition of the noise wavefield, (i.e. Rayleigh, Love, and body waves; see Bonnefoy-Claudet *et al.* 2006 for a review and Koper *et al.* 2010 for a global survey), making the interpretation of the H/V ratio difficult. The relationship between Rayleigh wave ellipticity (or Rayleigh wave H/V ratio) to the 1-D

shallow structure of the Earth, on the other hand, is well defined (Tanimoto & Rivera 2008). Extraction of Rayleigh wave ellipticity using 3-component array techniques has been shown to be quite reliable (Poggi & Fah 2010). Recently, multicomponent ambient noise cross-correlation techniques (NCC) have also been developed to obtain robust Rayleigh wave H/V amplitude ratio measurements (Lin & Schmandt 2014; Lin *et al.* 2014). This latest technique uses noise cross-correlations between station pairs to approximate the Rayleigh wave Green's functions between a station pair where one station is considered a virtual source and the other station is considered a receiver. The cross-correlations can then be used to make observations of Rayleigh wave H/V ratio by employing either a vertical or radial force at the virtual source, and measuring the amplitude ratio between radial and vertical component at the receiver.

While NCC has the advantage of isolating Rayleigh waves from ambient noise, interpretation of the result can be difficult if the

* Now at: ENSCO, Inc., 4849 North Wickham Road, Melbourne, FL 32940-7119, USA.
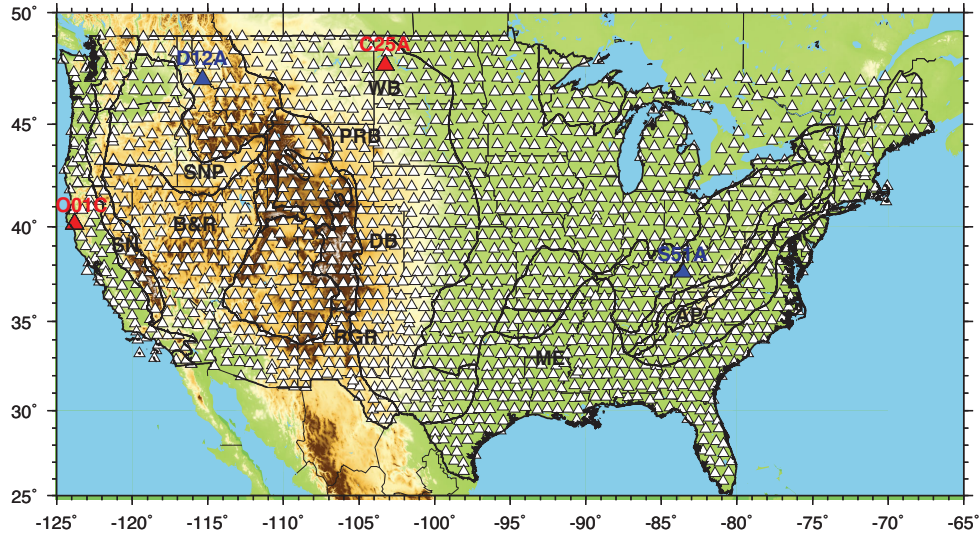
Figure 1. The Earthscope Transportable Array (TA) stations used in this study are represented by white triangles. The larger blue triangles represent stations D12A and S51A, used in Figs 2, 3, 4 and 10. The larger red triangles represent stations O01C and C25A, used in Fig. 9. The solid black lines represent major physiographic provinces across the U.S. (Fenneman 1917). Some major sedimentary basins are labeled within these geologic provinces, as well as notable regions discussed later in the paper (WB: Williston Basin; PRB: Powder River Basin; DB: Denver Basin; RGR: Rio Grande Rift; SNP: Snake River Plain; B&R: Basin and Range Province; SN: Sierra Nevada; ME: Mississippi Embayment; AP: Appalachians.
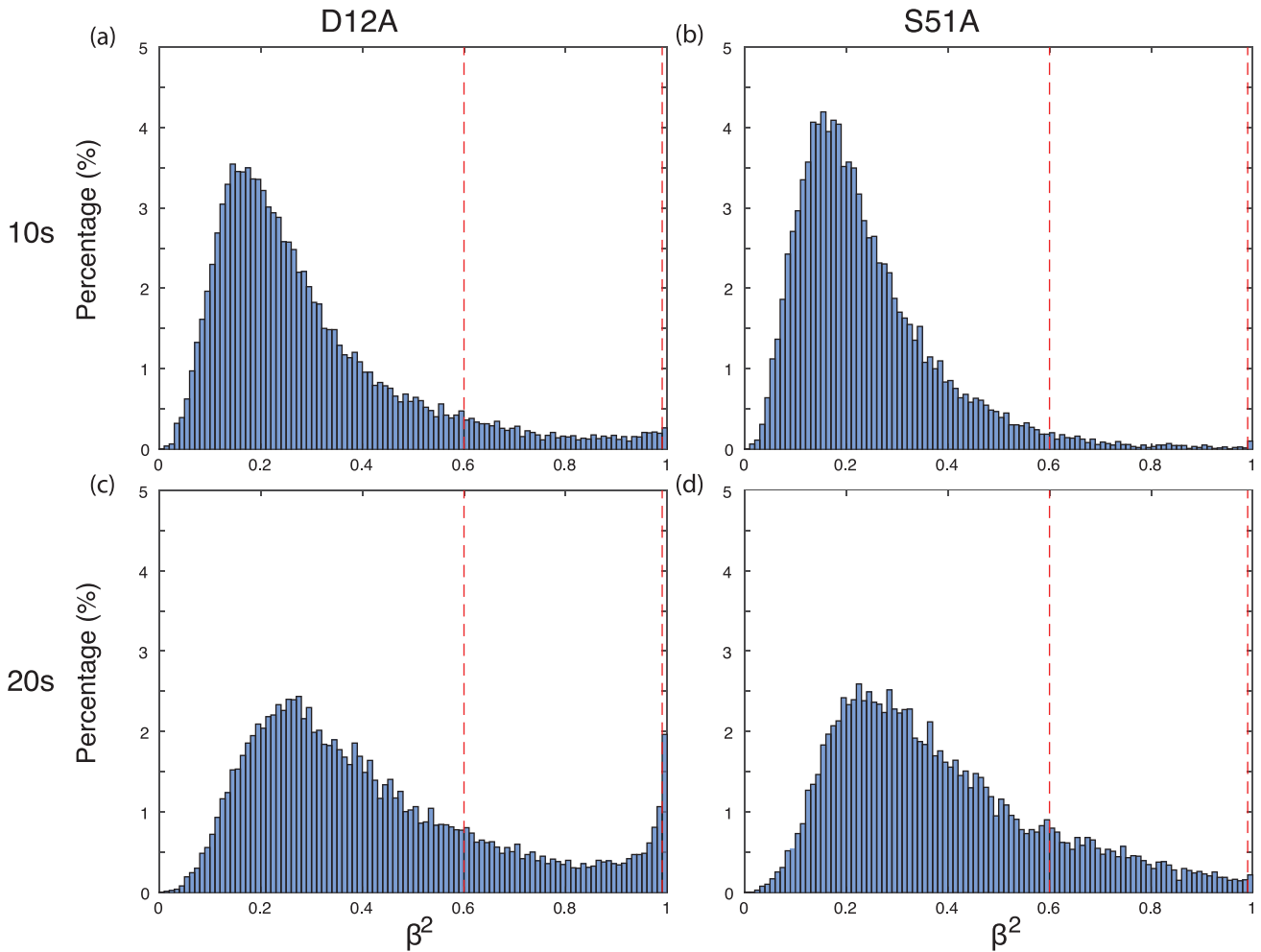
Figure 2. The distributions of β^2 for stations D12A and S51A at periods of 10 and 20 s. The portion of the distribution inside the vertical red dashed lines represent the values selected for further analysis. (a) Station D12A at 10 s. (b) Station S51A at 10 s. (c) Station D12A at 20 s. (d) Station S51A at 20 s.
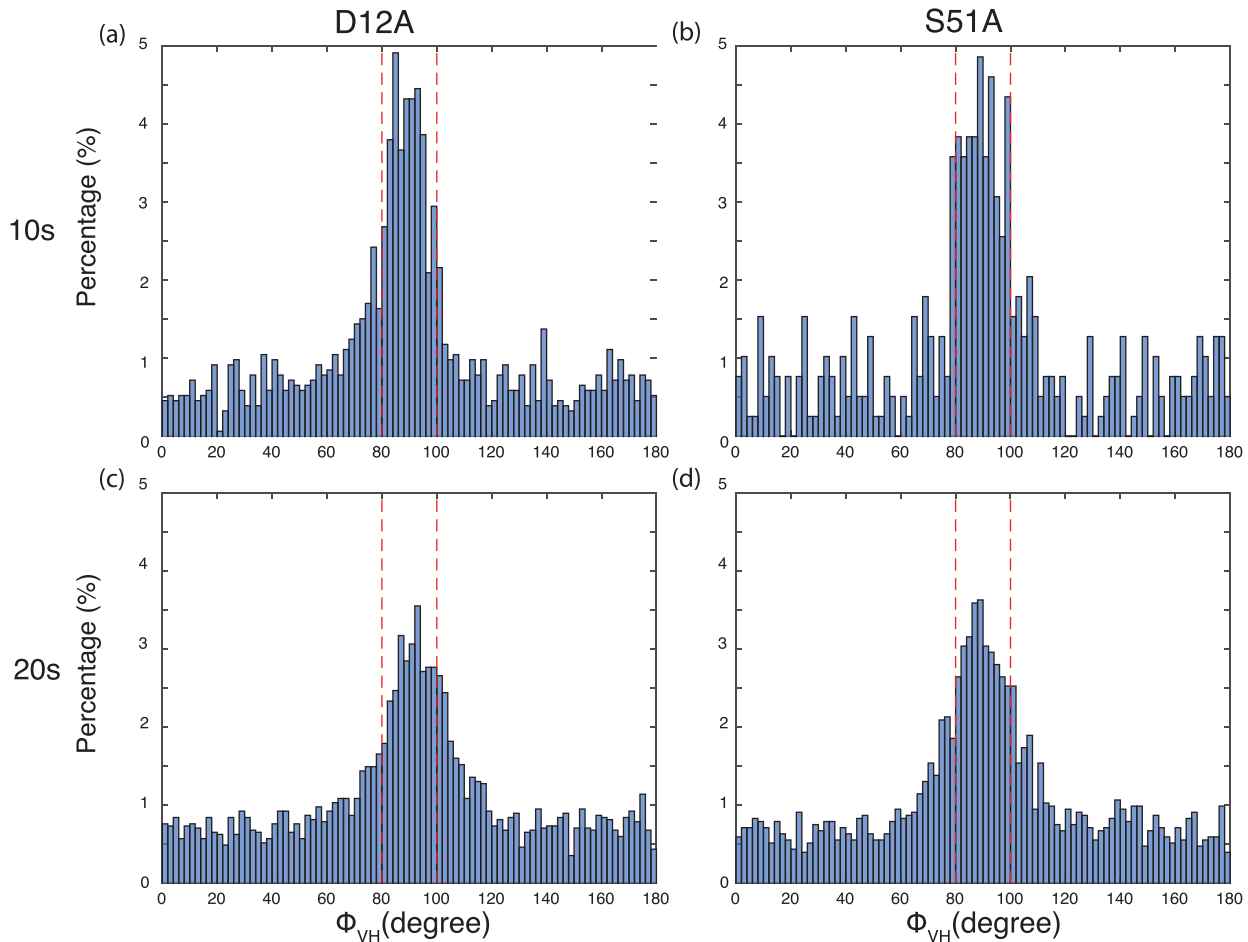
Figure 3. The distributions of Φ_{VH} for stations D12A and S51A after the data have passed the β^2 selection criteria for periods of 10 and 20 s. The portion of the distribution inside the vertical red dashed lines represent the values selected for further analysis. (a) Station D12A at 10 s. (b) Station S51A at 10 s. (c) Station D12A at 20 s. (d) Station S51A at 20 s.

noise field is not semi-diffusive. The far-field approximation helps to ensure a semi-diffusive noise field, but virtual source stations must be at least three wavelengths away from the target stations. The uncertainty of the measurement can also be high if there are not sufficient stations acting as virtual sources.

Single station methods have been proposed previously to determine Rayleigh wave ellipticity (Hobiger *et al.* 2009; Tanimoto *et al.* 2012) and have been applied to ambient seismic noise. Hobiger *et al.* (2009) relies on applying the random decrement technique, which emphasizes Rayleigh wave energy in the wavefield by stacking specially tuned signal windows, and calculates wave H/V ratios for the emphasized Rayleigh waves. Tanimoto *et al.* (2012) determined the phase-shift angle for the noise spectrum and calculates the Rayleigh wave H/V ratio for all hours that have a 90° phase differences between the vertical and horizontal components, and applied this technique for stations in Southern California. These methods perform well in identifying Rayleigh wave particle motion, but cannot determine the heterogeneity of the noise and the relative contribution of the Rayleigh wave energy. Single station methods have the advantage of utilizing a less sensitive to non-diffusive wavefield. However, the validity of these single station methods has not been rigorously tested, as the ground truth of the Rayleigh wave H/V ratio is not available.

In this study, we demonstrate a single station method for the determination of Rayleigh wave H/V ratios across the Earthscope

Transportable Array (Fig. 1) utilizing the Frequency Dependent Polarization Analysis (FDPA; Park *et al.* 1987; Koper & Hawley 2010; Koper & Burlacu 2015). We use FDPA to identify the dominant wave-type in the ambient seismic noise wavefield in 1-hr time windows, and extract H/V ratio measurements if that wave-type is indicative of Rayleigh wave particle motion. We perform this analysis over all available data for the Earthscope Transportable Array between 2004 and 2014. We compare the 8 to 30-s period results with the Rayleigh wave H/V ratio extracted from NCC (Lin *et al.* 2014) to evaluate the viability of the method. We show that with careful processing, the FDPA method can produce a result similar to the noise cross-correlation method across much of the USArray within the microseism frequency. We find the single station method has difficulty retrieving robust Rayleigh wave H/V ratios within major sedimentary basins where the noise wavefield is likely dominated by reverberating Love waves and tile noise as opposed to strongly polarized Rayleigh waves. While we find a consistent pattern between Rayleigh wave and NCC, the measurements above 10 s period are persistently slightly higher (~2 per cent), likely related to the greater horizontal noise due to other wave types (i.e. Love wave) or tilt noise. At 8 s period, the two H/V methods yield consistent results suggesting that the noise wavefield is dominated by Rayleigh waves. We also compare our results to classical noise spectrum H/V ratios (NSHV; e.g. Nakamura 1989) observed across the USArray to evaluate the relationship between the two often entangled
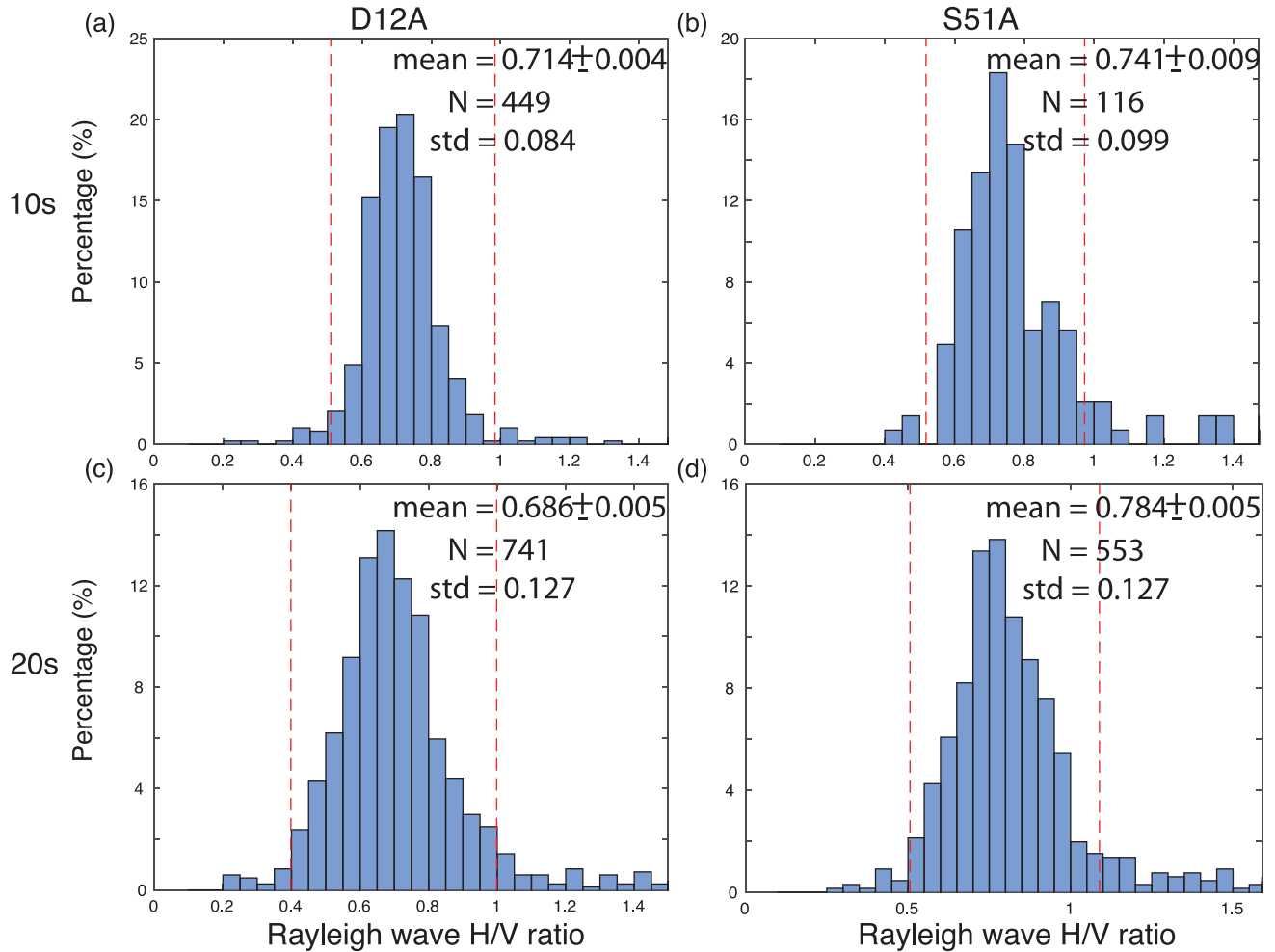
Figure 4. The distributions of H/V ratios for stations D12A and S51A after the β^2 and Φ_{VH} selection criteria have been implemented, at periods of 10 and 20 s. The portion of the distribution inside the vertical red dashed lines represent the values selected for which the mean H/V ratio and uncertainty is calculated. (a) Station D12A at 10 s. (b) Station S51A at 10 s. (c) Station D12A at 20 s. (d) Station S51A at 20 s.

measurements. While the general pattern is generally consistent between the two single-station measurements and the results agree well at 8 s period, the NSHV ratios are persistently more than 20 per cent higher than Rayleigh wave H/V ratio measurements 10 s period and above. This clearly demonstrates the effect of other signals (i.e. Love wave, body waves and tilt noise) on NSHV ratios.

2 METHODOLOGY

The following technique for determining Rayleigh-wave ellipticity, or Rayleigh-wave horizontal to vertical amplitude ratio (H/V ratio), is based on the approach described by Park *et al.* (1987). FDPA is the singular value decomposition of the spectral covariance matrix for a windowed segment of raw ambient seismic noise data. The resulting singular vectors and associated singular values can provide information on the composition of seismic noise, such as the degree of polarization, the mode of propagation, particle motion, and the direction of arrival. Assuming the dominant signal in the noise is Rayleigh wave energy, Rayleigh wave H/V ratio is calculated from the primary singular vector for a given frequency, by dividing the amplitude of the major axis of the horizontal ellipse by the amplitude of the vertical component of the same singular vector.

In this study, we first extract one hour of the 0.025 Hz sample rate three-component seismic data for all available USArray Transportable Array stations between 2004 and 2014. We then compute the spectral covariance matrices based on the method described by Sufri *et al.* (2014). For each component the instrument response is removed and a 0.002–10 Hz bandpass filter is applied. For all three components the segments are subdivided into 10 subwindows of 819.2 s length, with the windows overlapping by 62 per cent. The signal in each subwindow is detrended and tapered by a 10 per cent Hanning window, and converted to the frequency domain using fast Fourier transform (FFT). Once in the frequency domain, the 3-by-3 spectral covariance matrix is constructed by the multiplication of the three dimensional complex vector with its complex conjugate. The resulting matrix is a 3-by-3 and Hermitian, and each element is a function of frequency. The diagonal elements constitute the power spectra for the three components of motion. The spectral covariance matrices calculated for each subwindow are averaged to produce the one-hour spectral covariance matrix. Singular Value Decomposition (SVD) is then performed on the resulting matrix, where the primary singular vector and associated singular value are related to the dominant noise characteristics for that hour.

The degree of polarization (β^2), as defined by Samson (1983), is a useful measure for determining the heterogeneity of the ambient
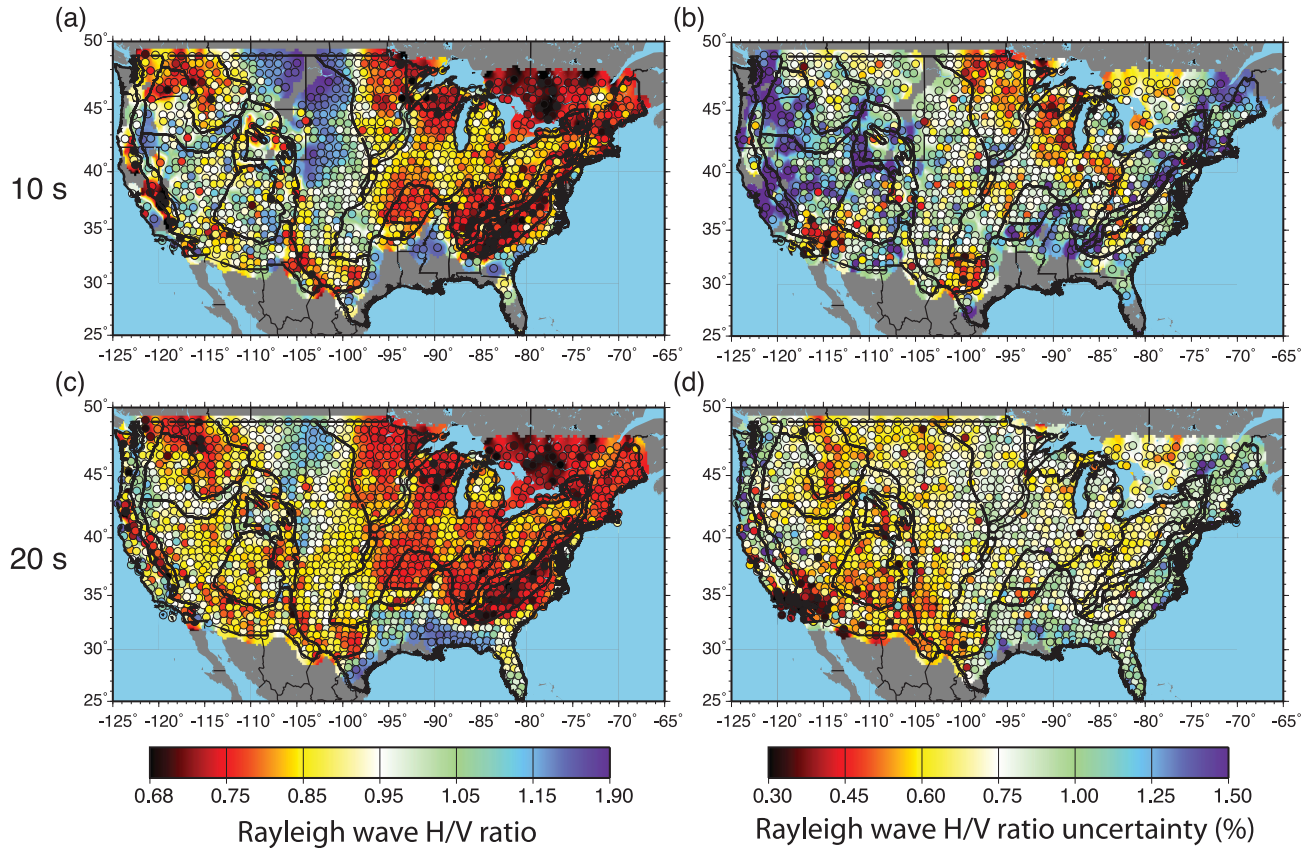
Figure 5. 10 s and 20 s Rayleigh wave H/V ratios observed across USArray using frequency dependent polarization analysis (FPDA). The Rayleigh wave H/V ratios for each station are plotted as colored circles. A Gaussian smoothing method is used to interpolate between stations and the smoothed map is plotted in the background. (a) Mean Rayleigh wave H/V ratio observations using FDPA for 10 s. (b) Rayleigh wave H/V ratio uncertainties for 10 s. (c) Mean Rayleigh wave H/V ratio observations using FDPA for 20 s. (d) Rayleigh wave H/V ratio uncertainties for 20 s.

noise field (Koper & Hawley 2010). This measurement is defined as follows:

$$\beta^2 = \frac{3tr\left(S^2\right) - \left[tr\left(S\right)\right]^2}{2\left[tr\left(S\right)\right]^2}, \quad (1)$$

where tr is the trace operator and S is the spectral covariance matrix. The interpretation of β^2 follows that if the recorded noise is completely disorganized, the three singular values will be equal and the resulting β^2 value will be 0. However, if the particle motion is recorded in a pure state, only one singular value will exist and the associated β^2 value will be 1. For our purposes, β^2 is calculated, and a cut-off value chosen so that we can select only the time windows that are closest to a pure state. Fig. 2 shows the β^2 distributions for stations D12A and S51A, respectively, at periods of 10 and 20 s. The cut-off value for β^2 in this study is 0.6; this was chosen to ensure that the primary singular value was fairly dominant, without eliminating vast amounts of data. An upper limit β^2 bound of 0.99 was also used to eliminate pure state signals that result from anomalous transient signals (e.g. instrument calibration).

We determine the horizontal phase angle, Φ_H and amplitude, A_H, from the major axis of the horizontal ellipse associated with the primary singular vector, as outlined by Park *et al.* (1987). The primary singular vector $\mathbf{Z}_p$, a complex unit vector described by amplitude and phase components ($A_z e^{-i\Phi_z}$, $A_x e^{-i\Phi_x}$, $A_y e^{-i\Phi_y}$),

is projected onto an ellipse in the horizontal plane, $\mathbf{Z}_H$. The major axis of the horizontal ellipse is determined by finding the maximum amplitude of $\mathbf{Z}_H$, which is equal to finding the maxima of:

$$a_H = \left[\left(A_x \cos\left(\omega t + \Phi_x\right)\right)^2 + \left(A_y \cos\left(\omega t + \Phi_y\right)\right)^2\right]^{\frac{1}{2}}. \quad (2)$$

The maxima of this expression is found when Φ_H, defined as ωt, takes the values of:

$$\Phi_H = -\left(\frac{1}{2}\right) arg\left(\left(A_x e^{-i\Phi_x}\right)^2 + \left(A_y e^{-i\Phi_y}\right)^2\right) + \frac{(l\pi)}{2}, \quad (3)$$

where l is an integer. Let l be the smallest integer that maximizes (2), and for which $\mathrm{Re}(A_z e^{-i\Phi_z}) < 0$. A_H is $\max(a_H)$.

The phase lag between the vertical and horizontal components of the primary singular vector can be found from the following equation:

$$\Phi_{VH} = \Phi_H - \Phi_z, \quad (4)$$

where Φ_z is the phase angle of the vertical component. With the freedom in integer l, the values of Φ_{VH} can be restricted to a range of $-90° \leq \Phi_{VH} \leq 90°$. For the purposes of this study the Φ_{VH} was recalculated such that $0° \leq \Phi_{VH} \leq 180°$, with a Φ_{VH} value of $90°$ is indicative of Rayleigh wave elliptical motion. Fig. 3 shows distributions of Φ_{VH} for stations D12A and S51A respectively, for periods of 10 and 20 s after the β^2 selection criteria had been applied.
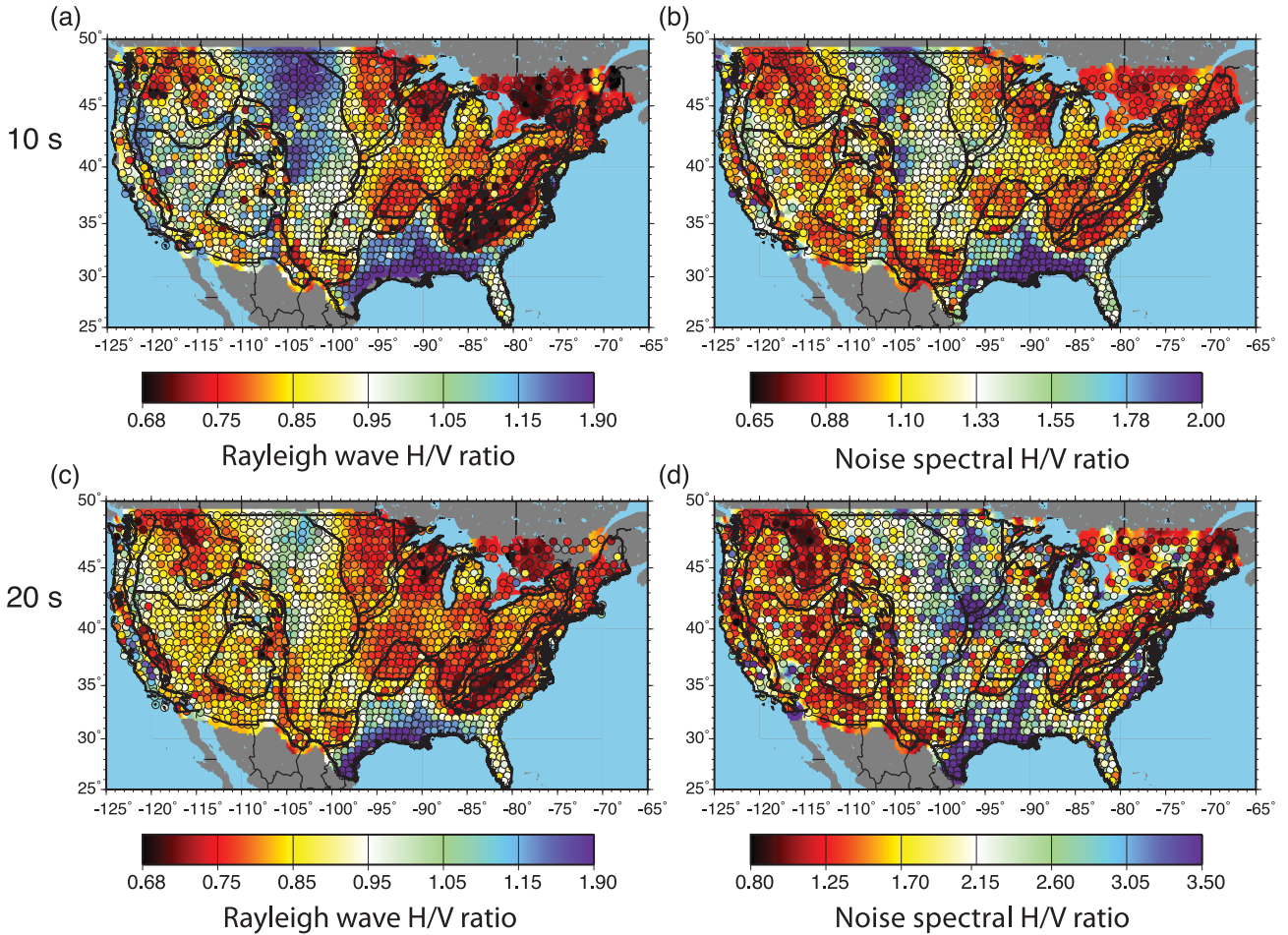
Figure 6. 10 and 20 s Rayleigh wave H/V ratios observed across USArray using the noise cross-correlation technique (NCC; Lin *et al.* 2014) and a traditional noise spectra H/V ratio method (NSHV; Nakamura 1989). (a) Rayleigh wave H/V ratio observation using NCC for 10 s. (b) NSHV observations for 10 s. (c) Rayleigh wave H/V ratio observation using NCC for 20 s. (d) NSHV observations for 20 s.

A cut-off criteria of $\pm 10°$ from $90°$ was used to select measurements that are likely associated with Rayleigh waves.

Once the β^2 and Φ_{VH} selection criteria have been implemented to identify Rayleigh-wave-like primary singular vectors, the Rayleigh wave H/V ratio is calculated as follows:

$$\frac{H}{V}\text{ratio} = \frac{A_H}{A_z}. \tag{5}$$

Fig. 4 shows the distributions of H/V ratio for the stations D12A and S51A at periods of 10 and 20 s. Note that the distribution of polarization analysis is slightly right-skewed. This may be due to the fact that even after that the β^2 and Φ_{VH} selection criteria has been implemented the primary singular vector is still contaminated with other wave types such as Love wave, body wave, and tilt noise. To obtain a more Gaussian-like distribution, we identify the main peak of the distribution, calculate the standard deviation to the left of that peak, and extract all data points that lie within 2 standard deviations of the main peak. The mean Rayleigh wave H/V ratio and the standard deviation of the mean are then calculated from this resampled distribution to determine the Rayleigh wave H/V ratio and its uncertainty at that station location. We remove all stations with the Rayleigh wave H/V ratio uncertainty larger than 2 per cent of the mean H/V ratio.

3 RESULTS AND DISCUSSION

3.1 Rayleigh wave H/V ratio measurements and maps

We present maps of mean Rayleigh wave H/V ratio and the standard deviation of the mean (uncertainty) for the Earthscope Transportable Array stations using the previously described Frequency Dependent Polarization Analysis at 10 and 20 sec periods (Fig. 5). A $0.5°$ Gaussian smoothing has been applied to each location and the interpolation placed on a $0.2° \times 0.2°$ grid in order to obtain smoothed maps. Considering the ~ 70 km station spacing, for each grid point the smoothing is constrained by observed measurements at the three to four nearest stations. To highlight the difference in values at each station, a circle representing each station filled with the Rayleigh wave H/V ratio value for that station is overlain onto the smoothed map.

At periods of 10 and 20 s, high Rayleigh wave H/V ratio values (Figs 5a and c) are found most prominently in major sedimentary basins, such as the Williston Basin, the Denver Basin, and the Mississippi Embayment. This is likely due to the large impedance contrast between the shallow sediments and the deeper crystalline bedrock, which the measurements are sensitive to (Lin *et al.* 2014). Rayleigh wave H/V ratios higher than 2 are observed at 10 s within part of the major sedimentary basins (e.g. Williston Basin), indicating that this period may be close to the resonant frequency of these
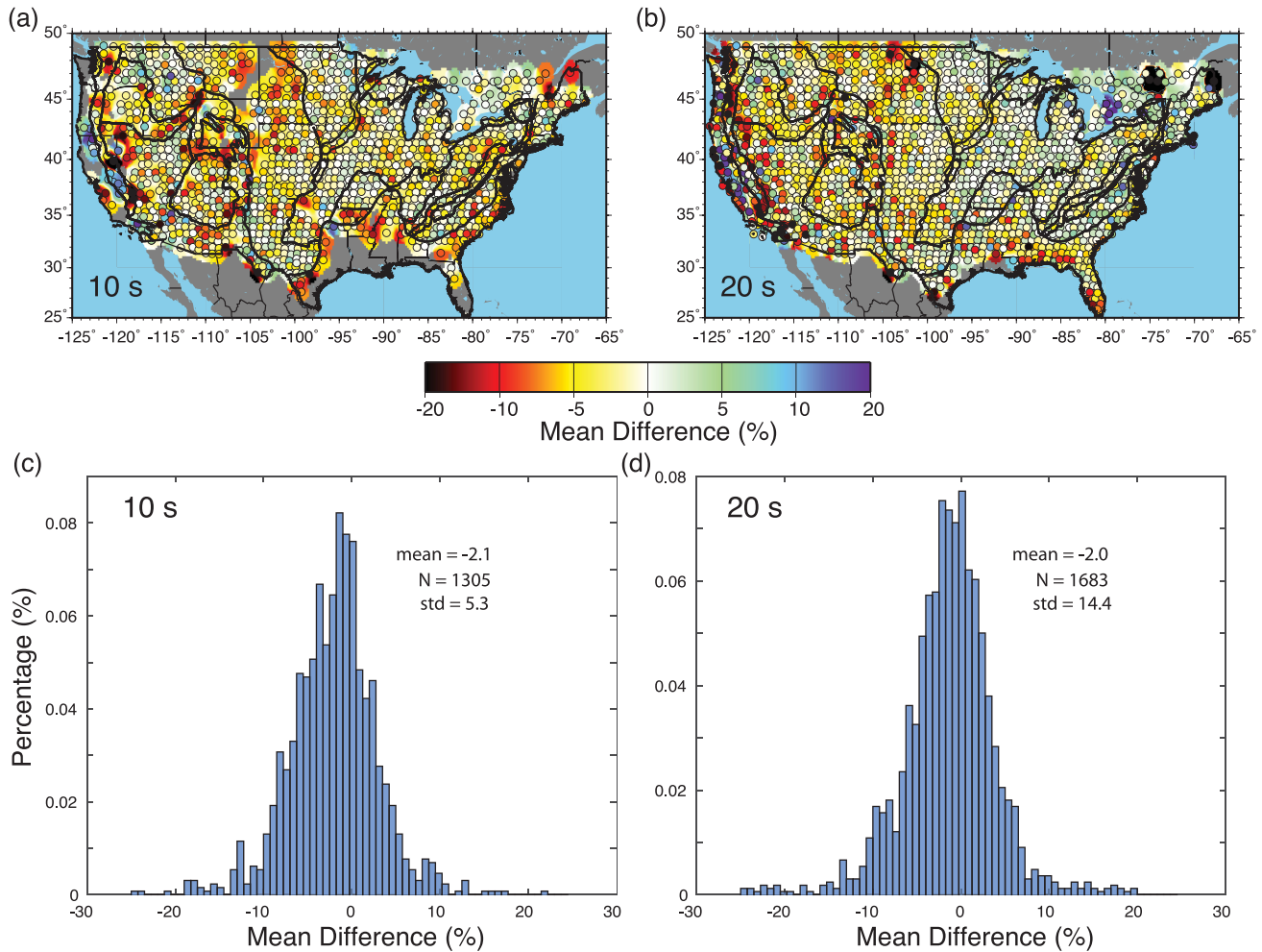
Figure 7. The differences in observed Rayleigh wave H/V ratios between the frequency dependent polarization analysis (FDPA) and noise cross-correlation methods (NCC; Lin *et al.* 2014) and their distributions for 10 and 20 s across USArray. Negative values indicate that the FDPA observation is the higher value. The H/V ratio differences for each station are plotted as colored circles. A Gaussian smoothing method is used to interpolate between stations. (a) Mean difference across USArray for 10 s. (b) Mean difference across USArray for 20 s. (c) Distribution of mean difference across USArray for 10 s. (d) Distribution of mean difference across USArray for 20 s.

sedimentary basins. Low Rayleigh wave H/V ratios are observed mostly in regions where crystalline rocks are exposed or very close to the surface. Both periods have several stations that do not pass our selection criteria (in particular at 10 s). The missing stations tend to be in regions of higher H/V ratios (>1.15), such as the major sedimentary basins. Within these structures, other wave types and tilt noise can be stronger and Rayleigh waves are no longer the dominant wave type (more discussion in Section 3.3).

While the standard deviation may be large for each station (e.g. Fig. 4), the uncertainty (standard deviation of the mean) is much smaller due to the large number of measurements. The uncertainties seem to be lower at 20 s across most of the array than at 10 s (Figs 5b and d), mostly because of a greater number of measurements passing the degree of polarization, β^2, selection criterion at 20 s compared to 10 s (Fig. 2). At longer periods, the noise is likely more coherent within each one hour time window, hence higher β values. The highest uncertainties for both periods appear to be in the sedimentary basins, including the Williston Basin, and the Mississippi Embayment, where there is more trapping of other energy types (e.g. Love waves) and tilt noise is more likely to be present. The uncertainties at both periods are particularly small for the stations in Southern California because these sta-

tions ran continuously throughout the USArray deployment, thus increasing the number of measurements and substantially decreasing the uncertainty.

3.2 Comparison with noise cross-correlation and traditional H/V spectra ratio

The Rayleigh wave H/V ratio values for periods of 10 and 20 s obtained in the previous noise cross-correlations study (Lin & Schmandt 2014) are shown in Figs 6(a) and (c) for comparison. The maps are very similar to the FDPA maps at the same periods with low Rayleigh wave H/V ratio values for mountains and high values for sedimentary basins. The NCC shows more stations than the FDPA method for both periods, as the method is less sensitive to local wavefield complexity. More specifically, Rayleigh waves can be isolated from other wave types using NCC even if Rayleigh waves are not the dominant wave type.

The difference in the FDPA and the NCC maps at 10 and 20 s periods and their associated histograms are shown in Fig. 7. The maps are smoothed and presented as described in the previous section. These maps are the percent difference of the FDPA analysis from
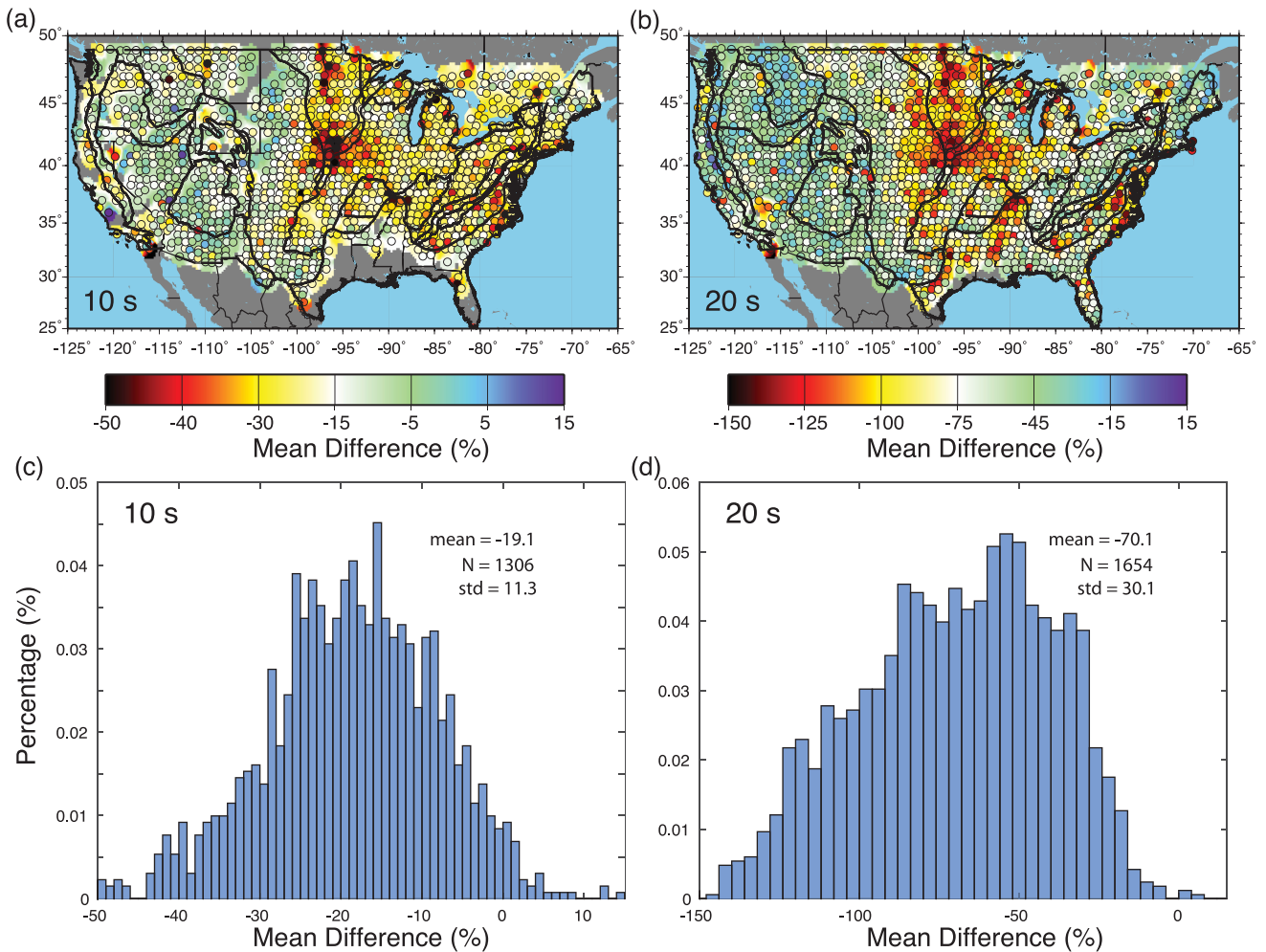
Figure 8. The differences in observed Rayleigh wave H/V ratios between the frequency dependent polarization analysis (FPDA) and a more traditional H/V spectra ratio approach (NSHV; Nakamura 1989) and their distributions for 10 and 20 s across USArray. Negative values indicate that the NSHV observation is the higher value. The H/V ratio differences for each station are plotted as colored circles. A Gaussian smoothing method is used to interpolate between stations. (a) Mean difference across USArray for 10 s. (b) Mean difference across USArray for 20 s. (c) Distribution of mean difference across USArray for 10 s. (d) Distribution of mean difference across USArray for 20 s.

the NCC, such that negative values on the map result in the FDPA analysis having a higher H/V ratio value. Overall the two methods compare very well, with the mean H/V ratio of the entire map for 10 and 20 s showing a disagreement of only ∼2 per cent. The overall agreement between the two methods suggests that reliable Rayleigh wave H/V ratios can be extracted from single station noise signals using FDPA. The persistent 2 per cent discrepancy, however, may represent a persistent error of the FDPA method owing to the un-perfected isolation of Rayleigh waves from other wave types. Note that Rayleigh wave H/V ratios determined from the NCC method could also be biased when noise sources are not homogeneously distributed.

For comparison we also calculate the average noise spectrum H/V ratio for each station in the USArray Transportable Array using a classical noise spectrum H/V ratio approach (NSHV; Nakamura 1989). The average H/V spectral noise ratio for each station was determined by calculating the geometric mean of the horizontal components of the spectral covariance matrix and dividing this value by the vertical component of the spectral covariance matrix for every hour available, and calculating the mean for all hours (Haghshenas *et al.* 2008). The standard deviation of the mean was also calculated for all H/V ratios for each station.

The NSHV ratios are displayed for 10 and 20 s (Figs 6b and d). Note that the two maps are shown with different color scales, with the 20 s map having a much higher range. The NSHV map at 10 s has a pattern somewhat similar to the Rayleigh wave H/V ratios of FDPA (Fig. 5a), although the noise spectrum H/V ratios are noticeably higher (∼20 per cent). This follows from the NSHV employing the entire noise wavefield, which includes Love waves and tilt noise that have greater horizontal displacement than Rayleigh waves, leading to a higher H/V ratio value. However, the general pattern of agreement suggests that Rayleigh waves are the dominant noise wave type at 10 s. At 20 s, while some similarity can still be observed, clear differences are also observed between the noise spectrum H/V ratios and Rayleigh wave H/V ratios. In particular, high NSHV ratios are observed near the central US whereas low Rayleigh wave H/V ratios are observed. Also, the noise spectrum ratios are about 100 per cent higher across the entire map. This suggests Rayleigh waves are no longer the dominant wave type of the ambient noise wavefield.

The difference in the FDPA analysis and the NSHV method at 10 and 20 s periods and their associated histogram are shown in Fig. 8. The values are the difference in the NSHV values from the FDPA values, such that negative values correspond to the NSHV
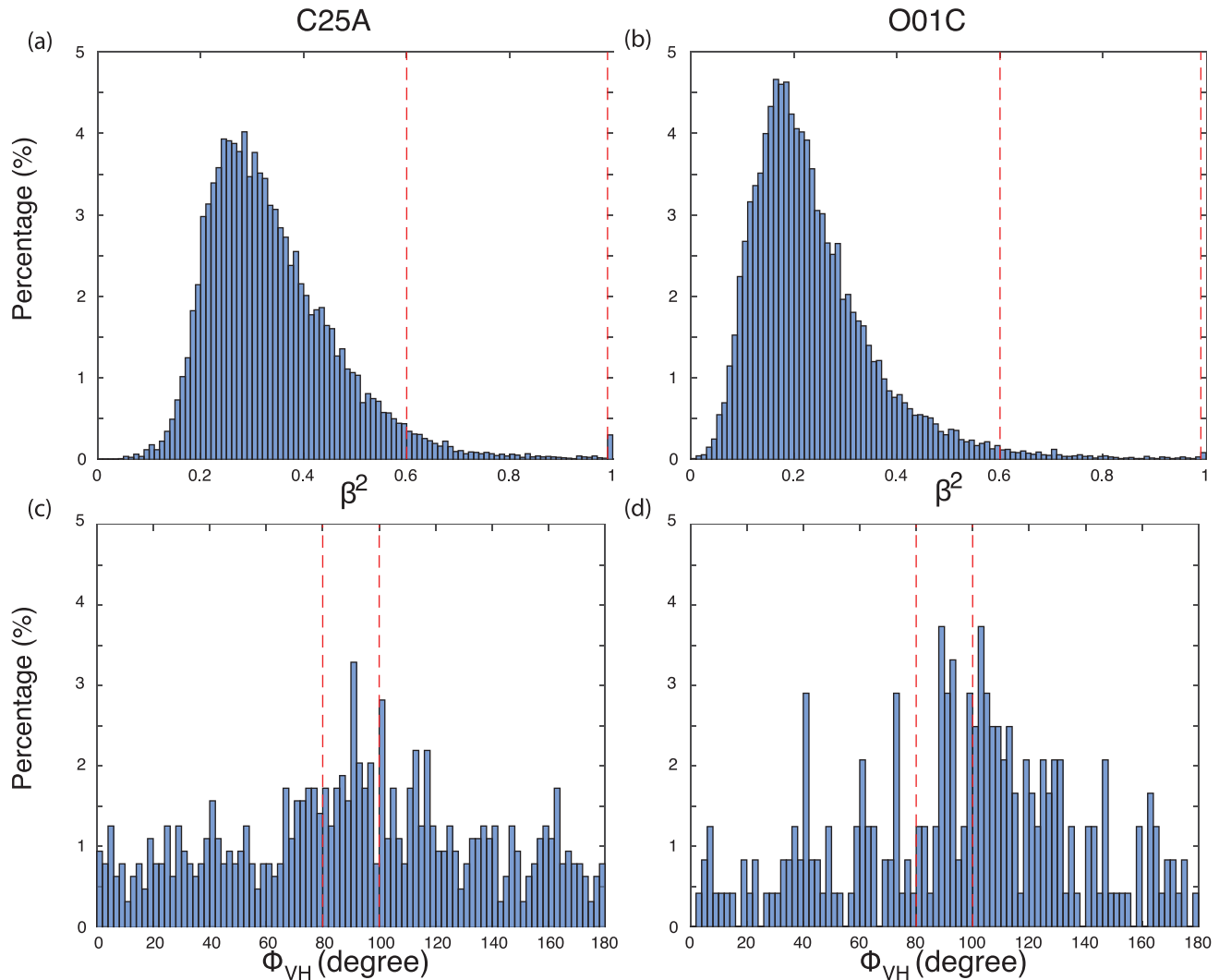
Figure 9. Examples of β^2 and Φ_{VH} distributions at 10 s for stations C25A and O01C, which are stations that did not pass the selection criteria. The vertical red dashed lines represent the same selection criteria used in Figs 2 and 3. (a) β^2 distribution for station C25A. (b) β^2 distribution for station O01C. (c) Φ_{VH} distribution for station C25A. (d) Φ_{VH} distribution for station O01C.

value being higher. Overall the NSHV method generates higher values than the FDPA method, owing to the inclusion of other wave types. There is a noticeable trend in both periods, in that the NSHV method generates the highest values in the Mid-West U.S. from the Canadian border to the Gulf Coast.

3.3 Potential problems with frequency dependent polarization analysis

The performance of the FDPA technique seems to be fairly dependent on the recording site geology. The regions of the map that seem to have the fewest number of data points passing the selection criteria include area of thick sedimentary basins, such as the Williston Basin in eastern Montana and western North Dakota, the Powder River Basin of northeastern Wyoming, the Denver basin of eastern Colorado, and the Mississippi embayment (Fig. 5). Fig. 9 shows the examples of β^2 and Φ_{VH} distributions for stations in these regions that did not pass the selection criteria (uncertainty larger than 2 per cent of the mean H/V ratio), and it is clearly seen that a large portion of the Φ_{VH} distributions do not lie within the selection bands (betwen 80 and 100 degree). Thick sedimentary layers

trap and scatter seismic energy, inducing a complicated, multistate wavefield (e.g. Benz & Smith 1988; Vidale & Helmberger 1988). The noise polarization analysis performed by Koper & Burlacu (2015) also suggests that wavefields in these basins are multistate and complex.

The NSHV maps also support this, which show greater values in thick sedimentary basins compared to Rayleigh wave H/V ratio results derived from NCC, owing to increased horizontal particle motion as compared to the vertical for the raw spectral data. Smaller-scale geologic features such as the Rio Grande Rift in central New Mexico and sedimentary basins in California also exhibit larger disagreements between FDPA and NCC, likely due to the trapping and amplification of seismic energy (Kagami *et al.* 1982; Yamanaka *et al.* 1993; Chapin & Cather 1994; Dolenc & Dreger 2005). FDPA is dependent on the wavefield present, and if that wavefield is complex and multistate the Rayleigh wave particle motion will be contaminated with other modes despite the β^2 and Φ_{VH} criteria. The selection criteria can be adjusted in these areas to insure that the particle motion is in a more pure state, but the number of successful measurements will likely be too small for a reliable H/V interpretation.
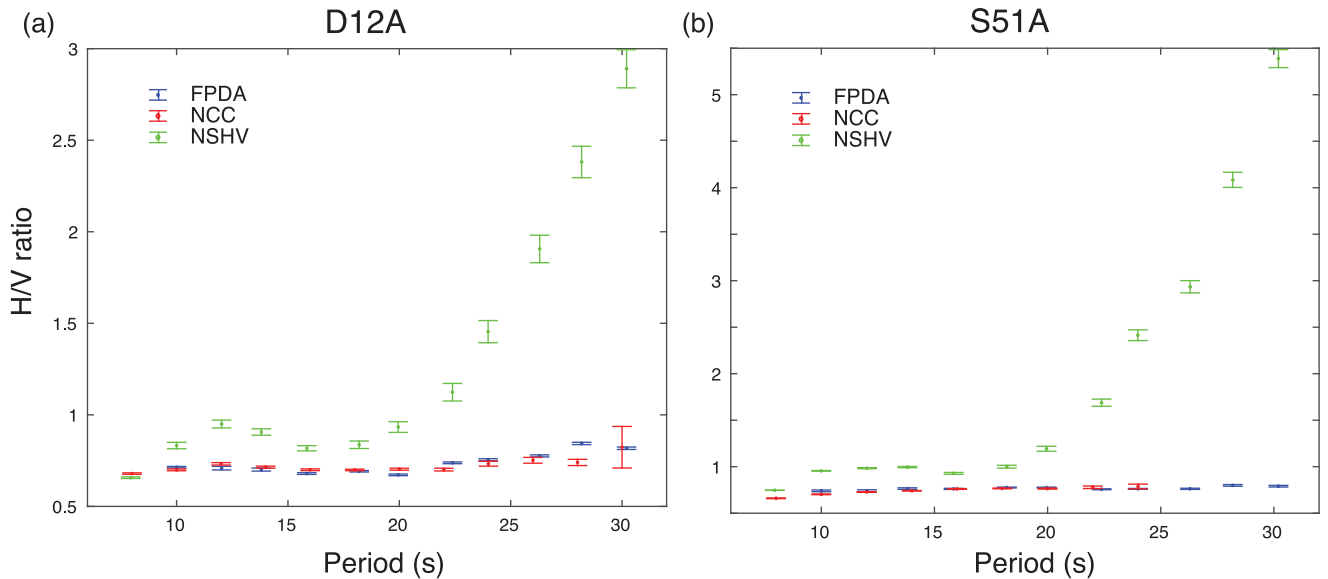
Figure 10. H/V ratio observations plotted against period for stations D12A and S51A. The blue points represent values from the frequency dependent polarization analysis (FPDA). The red points represent ratios calculated from the noise cross-correlations method (NCC; Lin *et al.* 2014). The green points represent observations utilizing the traditional H/V spectra ratio (NSHV; Nakamura 1989). Vertical bars represent the standard deviation of the mean.

FDPA appears to produce slightly higher H/V ratio values systematically than NCC (Fig. 7). This is likely due to the FDPA method sampling Rayleigh wave particle motion of a non-pure state, despite the β^2 and Φ_{VH} selection criteria, whereas the noise cross-correlations technique calculates H/V ratios from approximate Green's functions calculated between station pairs.

Anisotropy may also play a significant factor between these two methods. The work of Lin & Schmandt (2014) shows that for certain regions (in particular the Basin and Range Province, Sierra Nevada Mountain Range, Snake River Plain, and the Appalachian Mountain Range), Rayleigh wave H/V ratio measurements are strongly dependent on azimuth. This may be significant as FDPA can only sample azimuths for which the dominant wavefield is observed at the receiver, leading to a H/V ratio estimate that is systematically higher or lower if the source direction lies within a high or low Rayleigh wave H/V direction. This effect does not appear to be significant for the Basin and Range Province for 10 or 20 s where both methods show fairly good agreement (Fig. 7), but it may play a part as to why the Sierra Nevada and the Snake River Plain regions have larger disagreement.
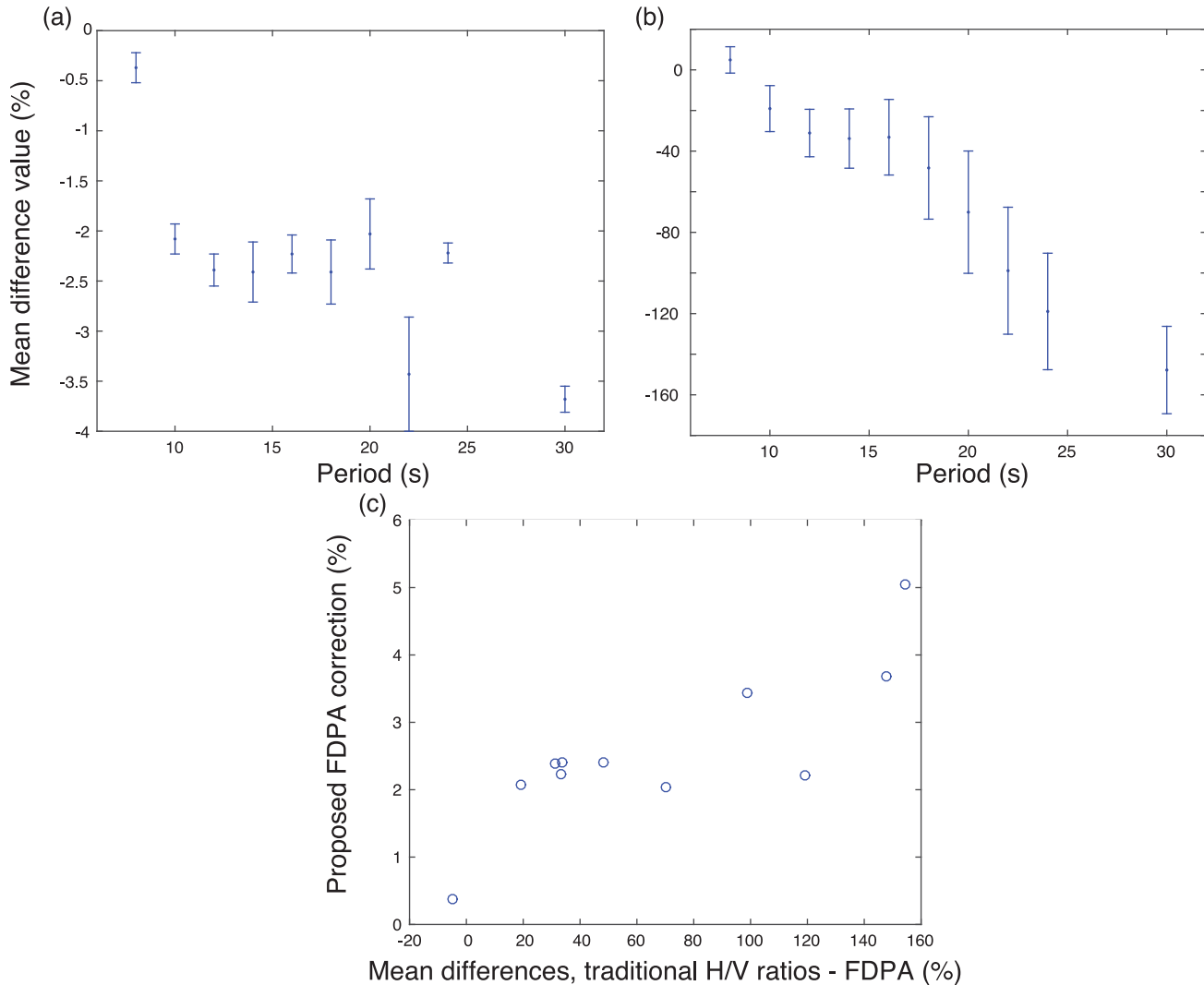
3.4 Period dependence of frequency dependent polarization analysis

The FDPA method has the best agreement with NCC and NSHV ratios near the secondary microseism period (~8 period) (Figs 10 and 11). Studies have shown that the Earth's ambient noise wavefield is especially strong within the microseism band (Peterson 1993; McNamara & Buland 2004), where theoretical studies have shown that the generation of Rayleigh waves from the ocean within this band (Tanimoto 2007; Ardhuin *et al.* 2011). At 8 s, Rayleigh waves are likely the overwhelming energy in ambient seismic noise and hence the H/V ratios from the three methods are in good agreement. Fig. 10 shows the H/V ratio measurements vs period for all three methods and their uncertainties at stations D12A and S51A. This figure illustrates the overall agreement with FDPA and the NCC

method between 8 and 30 s periods and at the same time shows how the NSHV ratios approaches the Rayleigh wave H/V ratios at 8 s, indicating the highest relative portion of Rayleigh wave energy.

Further evidence to support this period dependence is the mean differences between the FDPA method and NSHV (Fig. 11b), which displays the smallest relative difference between the three methods across the entire USArray at 8 s period. Within the microseism band (between 6 and 30 se period) the NCC method and the FDPA are generally agreed within 2 per cent but the discrepancy increases with the period (Fig. 11a). This suggests Rayleigh wave is the dominant noise wave type within the microseism band and FDPA can successfully isolate the Rayleigh waves. Above the microseism band however, other wave types and tilt noise are likely more important and FDPA is not effective in isolating Rayleigh waves as Rayleigh waves are no longer the dominant signal. As NSHV ratios are even more sensitive to the presence of other wave types, the increasing discrepancy with period clearly demonstrates the reduction of relative Rayleigh wave energy. For using a single station method to evaluate Rayleigh wave H/V ratios when NCC is not applicable, we recommend using the comparison between FDPA and NSHV to evaluate the dominance of Rayleigh waves and evaluate potential systematic error (Fig. 11c).

While NCC has the advantage of isolating pure Rayleigh waves, the method is only accurate when the noise wavefield is semi-diffusive. Moreover, the method only works when reliable Rayleigh wave signals can be identified. The near 70 km average spacing between USArray stations effectively limits the application to study Rayleigh wave H/V ratios below 8 s period band as waves attenuated and scattered during propagation. While the single station FPDA method can potentially be used to better extract higher frequency Rayleigh wave H/V ratios, the noise may be too transient in nature that the particle motion is not dominated by one single state continuously over a 1-hour segment. It may be possible to extract reliable Rayleigh wave particle motion information with FDPA by reprocessing the data with smaller time windows, such that the gain in accuracy over conventional H/V spectral ratio techniques can be

Figure 11. (a) The mean differences for all Rayleigh wave H/V ratio observations between the frequency dependent polarization analysis (FPDA) and the noise cross-correlations methods (NCC; Lin *et al.* 2014) plotted against all available periods between 8 and 100 s. Negative values indicate that the frequency dependent polarization analysis observation is the systematically higher value. The vertical bars represent the standard deviation of the mean. (b) The mean differences for all Rayleigh wave H/V ratio observations between FPDA and a more traditional H/V spectra ratio approach (NSHV; Nakamura 1989) plotted against all available periods between 8 and 100 s. Negative values indicate that the NSHV observation is the higher value. The vertical bars represent the standard deviation. (c) The FDPA correction needed, based on the observed differences between the NSHV ratio and the FDPA Rayleigh wave H/V ratio. For example, a 20 per cent mean difference between the NSHV ratio would result in a FDPA reduction of ∼2 per cent.

extended down to periods shorter than 8 s, however that is outside of the scope of the current study.

4 CONCLUSIONS

We developed and implemented a new single station method for the extraction of Rayleigh wave H/V ratios from ambient seismic noise. It is an extension of the method of Park *et al.* (1987), and uses the singular value decomposition of a 3-by-3 Hermitian, spectral covariance matrix. It differs from other single station methods that have been recently proposed (Hobiger *et al.* 2009; Poggi & Fah 2010; Tanimoto *et al.* 2012) in that it can determine how dominate and pure of state the Rayleigh wave particle motion is in the ambient noise by a comparison of the primary singular value to the two lesser singular values. We applied this technique over all available data from the Earthscope Transportable Array between 2004 and 2014, and compared the 8 to 30 second period results with the

Rayleigh wave H/V ratio extracted from noise cross-correlations (Lin *et al.* 2014) to check the method's viability. We also compared our results to H/V spectral noise ratios (Nakamura 1989) observed across the USArray to evaluate the relationship between the two measurements.

We showed that with careful processing, the FDPA method can produce a result similar to the NCC method across much of the USArray within the microseism period band of 8 to 24 s. This approach can be used in future studies for which a dense array cannot be deployed and the shallow structure of the area would like to be known. While no persistent error is observed at 8 s, the FDPA H/V ratio measurements above the 10 s period is slightly, though consistently, higher than the result from NCC. Because of this systematic bias the standard deviation of the mean of the result may be underestimated. We recommend correcting this bias based on the comparison of FDPA Rayleigh wave H/V ratios and the NSHV ratios when the noise cross-correlations method cannot be implemented. For example, a 20 per cent difference between the

NSHV ratio and the FDPA observation would result in a ∼2 per cent reduction of the FDPA Rayleigh wave H/V ratio (Fig. 11c). We find the single station method has difficulty retrieving robust Rayleigh wave H/V ratios within major sedimentary basins where the noise wavefield is likely not Rayleigh wave dominated. Disagreement between FDPA and the NCC method may also be due to FDPA sampling Rayleigh wave energy predominately from azimuths in the high or low Rayleigh wave H/V direction (Lin & Schmandt 2014).

REFERENCES

Ardhuin, F., Stutzmann, E., Schimmel, M. & Mangeney, A., 2011. Ocean wave sources of seismic noise, *J. geophys. Res.,* **166,** C09004, doi:10.1029/2011JC006952.

Benz, H.M. & Smith, R.B., 1988. Elastic-wave propagation and site amplification in the Salt Lake Valley, Utah, from simulated normal faulting earthquakes, *Bull. seism. Soc. Am.,* **78,** 1851–1874.

Bonila, L.F., Steidl, J.H., Lindley, G.T., Tumarkin, A.G. & Archuleta, R.J., 1997. Site amplification in the San Fernando Valley, California: variability of site-effect estimation using the *S*-wave, code, and H/V methods, *Bull. seism. Soc. Am.,* **87,** 710–730.

Bonnefoy-Claudet, S., Cotton, F. & Bard, P.-Y., 2006. The nature of the seismic noise wave field and its implication for site effects studies: a literature review, *Earth Sci. Rev.,* **79**(3–4), 205–227.

Chapin, E.C. & Cather, S.M., 1994. Tectonic setting of the axial basins of the northern and central Rio Grande rift, *GSA Spec. Pap.,* **291,** 5–26.

Dolenc, D. & Dreger, D., 2005. Microseims observations in the Santa Clara Valley, California, *Bull. seism. Soc. Am.,* **95,** 1137–1149.

Fenneman, N.M., 1917. Physiographic subdivisions of the United States, *Proc. Natl. Acad. Sci. U.S.A.,* **3**(1), 17–22.

Field, E. & Jacob, K., 1993. The theoretical response of sedimentary layers to ambient seismic noise, *Geophys. Res. Lett.,* **20,** doi:10.1029/93GL03054.

Haghshenas, E., Bard, P.-Y. & Theodulidis, N., 2008. Empirical evaluation of microtremor H/V spectral ratio, *Bull. Earthq. Eng.,* **6,** 75–108.

Hobiger, M., Bard, P.-Y., Cornou, C. & Le Bihan, N., 2009. Single station determination of Rayleigh wave ellipticity by using the random decrement technique (RayDec), *Geophys. Res. Lett.,* **43,** doi:10.1029/2009GL038863.

Kagami, H., Duke, C.M., Liang, G.C. & Ohta, Y., 1982. Observation of 1 to 5 s microtremors and their application to earthquake engineering. Part II. Evaluation of site effect upon seismic amplification due to extremely deep soil deposits, *Bull. seism. Soc. Am.,* **72,** 987–998.

Konno, K. & Ohmachi, T., 1998. Ground-motion characteristics estimated from spectral ratio between horizontal and vertical components of microtremor, *Bull. seism. Soc. Am.,* **88,** 228–241.

Koper, K.D. & Burlacu, R., 2015. The fine structure of double-frequency microseisms recorded by seismometers in North America, *J. geophys. Res.,* **120,** 1677–1691.

Koper, K.D. & Hawley, V.L., 2010. Frequency dependent polarization analysis of ambient seismic noise recorded at a broadband seismometer in the central United States, *Earth Sci.,* **23**(3–4), 439–447.

Koper, K.D., Seats, K. & Benz, H.M., 2010. On the composition of Earth's short period seismic noise field, *Bull. seism. Soc. Am.,* **100,** 606–617.

Lin, F.-C. & Schmandt, B., 2014. Upper crustal azimuthal anisotropy across the contiguous U.S. determined by Rayleigh wave ellipticity, *Geophys. Res. Lett.,* **41,** doi:10.1002/2014GL062362.

Lin, F.-C., Tsai, T.C. & Schmandt, B., 2014. 3-D crustal structure of the western United States: application of Rayleigh-wave ellipticity extracted from noise cross-correlations, *Geophys. J. Int.,* **198**(2), 656–670.

McNamara, D.E. & Buland, R.P., 2004. Ambient noise levels in the continental United States, *Bull. seism. Soc. Am.,* **94**(4), 1517–1527.

Nakamura, Y., 1989. A method for dynamic characteristics estimation of subsurface using microtremor on the ground surface, *Q. Rep. Railw. Tech. Res. Inst.,* **30,** 25–30.

Park, J., Vernon, F.L. & Lindberg, C.R., 1987. Frequency dependent polarization analysis of high-frequency seismograms, *J. geophys. Res.,* **92**(12), 664–674.

Parolai, S., Bormann, P. & Milkereit, C., 2002. New relationships between V_s, thickness of sediments, and resonance frequency calculated by the H/V ratio of seismic noise for the Cologne area, *Bull. seism. Soc. Am.,* **92,** 2521–2527.

Peterson, J., 1993. Observation and modeling of seismic background noise. U.S. Geol. Surv. Tech. Rep., 93–322, 1–95.

Poggi, V. & Fah, D., 2010. Estimating Rayleigh wave particle motion from three-component array analysis of ambient vibrations, *Geophys. J. Int.,* **180,** 251–267.

Riepl, J., Bard, P.-Y., Hatzfeld, D., Papaioannou, C. & Nechtschein, S., 1998. Detailed evaluation of site-response estimation methods across and along the sedimentary valley of volvi (EURO-SEISTEST), *Bull. seism. Soc. Am.,* **88,** 488–502.

Samson, J.C., 1983. The reduction of sample-bias in polarization estimators for multichannel geophysical data with anisotropic noise, *Geophys. J. Royal Astron. Soc.,* **75,** 289–308.

Sufri, O., Koper, K.D., Burlacu, R. & de Foy, B., 2014. Microseisms from Superstorm Sandy, *Earth planet. Sci. Lett.,* **402,** 324–336.

Tanimoto, T., 2007. Excitation of microseism, *Geophys. Res. Lett,* **34,** L05308, doi:10.1029/2006GL029046.

Tanimoto, T. & Rivera, L., 2008. The ZH ratio method for long-period seismic data: sensitivity kernels and observational techniques, *Geophys. J. Int.,* **172,** 187–198.

Tanimoto, T., Yano, T. & Hakamata, T., 2012. An approach to improve Rayleigh-wave ellipticity estimates from seismic noise: application to the Los Angeles Basin, *Geophys. J. Int.,* **193,** 407–420.

Vidale, J.E. & Helmberger, D.V., 1988. Elastic finite-difference modeling of the 1971 San Fernando, California earthquake, *Bull. seism. Soc. Am.,* **78,** 122–141.

Yamanaka, H., Dravinski, M. & Kagami, H., 1993. Continuous measurements of microtremors on sediments and basement in Los Angeles, California, *Bull. seism. Soc. Am.,* **83,** 1595–1609.